LAWRENCE
LIVERMORE
NATIONAL
LABORATORY

LLNL-JRNL-533771

CO oxidation on nanoporous gold: a combined TPD and XPS study of active catalysts

S. Roehe , V. Zielasek, A. Schaefer, A. Wittstock, K. Frank, A. Rosenauer, M. Baeumer

February 28, 2012

Surface Science

Disclaimer

This document was prepared as an account of work sponsored by an agency of the United States government. Neither the United States government nor Lawrence Livermore National Security, LLC, nor any of their employees makes any warranty, expressed or implied, or assumes any legal liability or responsibility for the accuracy, completeness, or usefulness of any information, apparatus, product, or process disclosed, or represents that its use would not infringe privately owned rights. Reference herein to any specific commercial product, process, or service by trade name, trademark, manufacturer, or otherwise does not necessarily constitute or imply its endorsement, recommendation, or favoring by the United States government or Lawrence Livermore National Security, LLC. The views and opinions of authors expressed herein do not necessarily state or reflect those of the United States government or Lawrence Livermore National Security, LLC, and shall not be used for advertising or product endorsement purposes.

CO oxidation on nanoporous gold: a combined TPD and XPS study of active catalysts

Sarah Röhe[1], Volkmar Zielasek[1], Andreas Schaefer[1], Arne Wittstock[1],
Kristian Frank[2], Andreas Rosenauer[2], Marcus Bäumer[1]

1) University of Bremen, Institute of Applied and Physical Chemistry, Leobener Str. NW 2, 28359 Bremen, Germany

2) University of Bremen, Institute of Solid State Physics, Otto-Hahn-Allee 1, 28359 Bremen, Germany

Abstract

Disks of nanoporous gold (np-Au), produced by leaching of silver from AgAu alloy and prepared as active catalysts for CO oxidation in a continuous-flow reactor, were investigated in detail by x-ray photoelectron spectroscopy and temperature-programmed desorption spectroscopy in ultrahigh-vacuum. Np-Au exhibits several oxygen species on and in the surface: Chemisorbed oxygen (O_{act}), probably generated at residual silver sites at the surface, is readily available after np-Au preparation and consumed by CO oxidation. It can be replenished on activated np-Au by exposure to O_2. In addition, strongly bound oxygen, probably at subsurface sites, is present as a major species and not consumed by CO oxidation. Pronounced CO desorption at temperatures above 200 K observed after exposing np-Au to CO at 105 K indicates an additional, more stable type of CO binding sites on np-Au as compared to pure gold. Only CO at these binding sites is consumed by oxidation reaction with O_{act}. It is proposed that the presence of strongly bound subsurface oxygen stabilizes CO adsorption on np-Au, thereby being as crucial for the observed catalytic activity of np-Au as residual silver.

Introduction

More than twenty years ago, the discovery of high catalytic activity of oxide-supported nanosized gold particles for CO oxidation spurred research efforts that, in the meantime, have led to prospects of profitable applications of gold as heterogeneous catalyst for gas-phase reactions, e.g., in automotive exhaust control or for selective hydrocarbon oxidation towards commodity chemicals such as propylene oxide. The fact that gold catalysts are particularly efficient for oxidation reactions at relatively low temperature came as a surprise because the noblest of all metals has, above all, a low affinity towards molecular oxygen[1,2]. Neither molecular nor dissociative chemisorption of O_2 on planar gold surfaces, not even in the presence of steps and kinks, have been observed at temperatures from 100 to 800 K, the relevant range for catalytic activity[3-5]. In fact, the basic mechanism of oxygen supply in gold-catalyzed CO oxidation has been debated from the early experiments up to now.

In the case of supported gold nanoparticles, it has been proposed that adsorption and dissociation of O_2 may occur on low-coordinated gold atoms which are abundant as a consequence of the small size, or is promoted by quantum size effects[6-8] which render the gold nanoparticles non-metallic. Another suggestion is that O_2 dissociation involves the reducible oxide support (in particular titania) and oxygen delivery proceeds across the interface between the particle and the support[9,10]. However, meanwhile catalytic activity has also been observed for unsupported gold powder [11], gold nanotubes embedded in polycarbonate membranes[12] and, in particular, monolithic nanoporous gold (np-Au)[13,14]. Latter experiments emphasized the notion that high catalytic activity of gold for CO oxidation may require neither any support nor finely dispersed particles.

Np-Au has a sponge-like structure, consisting of interconnected polycrystalline ligaments with fairly uniform diameters typically on the order of some ten nanometers. Besides CO oxidation, the material has been demonstrated to catalyze several reactions, such as selective gas-phase oxidative coupling of methanol[15], liquid-phase oxidation of glucose[16], electrochemical oxidation of methanol[17] and O_2 reduction in fuel cell applications[18]. Beyond that, np-Au has interesting chemo-mechanical properties and can potentially be used in sensor[19] and actuator[20] applications.

In the present study, temperature-programmed desorption (TPD) and x-ray photoemission spectroscopy (XPS) in ultra-high vacuum (UHV) were employed to gain more detailed insight into the mechanisms and surface species relevant for the catalytic performance of np-Au with respect to CO oxidation. Typically, these surface science techniques are employed at single

crystal surfaces, prepared clean to act as model for the catalyst surface. In the case of gold, however, techniques that circumvent the high activation barrier of O_2 dissociation such as ozone-treatment[21,22], oxygen plasma[23,24], sputtering with oxygen ions[25-27] or electron-induced dissociation of a condensed layer of O_2[27] are indispensable to generate adsorbed atomic oxygen on extended single-crystal surfaces, even when they exhibit a high density of low-coordinated sites as given in case of high-index surfaces or generated by ion bombardment.

In contrast, it is evident that in the case of np-Au there must be sustained O_2 dissociation at the surface for oxidation reactions. Experimentally, it has been proven that traces of silver as residues from the production process of np-Au are important for the catalytic activity and tune the tendency of np-Au for partial or total oxidation, implying that Ag is involved in the supply of atomic oxygen.[28 29] A recent theoretical study indeed suggested that the silver residues increase the adsorption energy of O_2 and lower its dissociation energy.[30,31]. Because of the complex surface chemistry rendering the high activity for CO oxidation, we refrained from studying model systems based on single crystal gold surfaces, but employed TPD and XPS *directly* at np-Au samples which had been proven as active catalysts for CO oxidation in a continuous-flow reactor.

Investigating adsorption and reaction on porous materials by surface science techniques in UHV holds several challenges. Only the relatively small outer, i.e., visible part of the large specific surface area of the sample disks is accessible to techniques like XPS or infrared absorption spectroscopy which provide information about chemical surface states or adsorbed species and reaction intermediates. TPD, in contrast, routinely employed to identify reaction products, may be dominated by the surface area of the inner pores. In the following, we will demonstrate that despite these challenges and despite the complexity of the material under investigation, some clear conclusions can be drawn which reveal that, besides silver, in particular various resident oxygen species on and in the surface play a role for the unique catalytic properties of np-Au. Not all of these oxygen species that interact with CO are active in such a way that they are consumed in the oxidation reaction.

Experimental section

Np-Au was prepared by selective electrolytic dissolution of Ag from AuAg alloy disks (30 at% Au, 70% Ag), each disk with a diameter of 4.9 mm and a thickness of 0.2 mm. The dealloying process was carried out in 5-M nitric acid at room temperature with a typical three-

electrode setup. The sample (working electrode) was mounted on a gold-wire formed as a basket. The alloy disk was set to an electrochemical potential of 60 mV with respect to a Pt-foil reference electrode, a Pt foil was also deployed as counter electrode (Potentiostat, Wenking POS 88, BANK Electronics) for 32 - 48 hours of etching. Under the chosen conditions, 1 - 5 at.% Ag remain in the bulk.

The resulting material has pores and ligaments with diameters of typically 50 - 100 nm (see Fig. 1 for scanning electron and transmission electron micrographs (SEM, TEM) of np-Au ligaments). The specific surface area of np-Au, as determined by BET analysis of N_2 adsorption, is ~4 m²/g from which an inner surface area of 0.1 m² can be calculated for a np-Au sample, i.e., ~ 2500 times larger than the geometric surface of the sample disk.

Activation of the as-prepared samples for CO oxidation proceeded in a fixed-bed reactor at ambient pressure and 350 K in a continuous flow of 2 mL/min CO and 5 mL/min O_2 (using He as carrier and a total stream of 50 mL/min). After few hours (< 10 h), the samples showed catalytic activity by steady state conversion of CO. Out of the reactor, the samples were immediately clamped by Mo wire onto a plane Omicron-type sample holder made of Mo (Omicron-type) and transferred into ultrahigh-vacuum.

The UHV system (base pressure < 10^{-10} mbar) comprised a differentially pumped quadrupole mass spectrometer (Hiden) for TPD and an X-ray photoelectron spectroscopy unit (Leybold EA 10 plus and VG dual anode X-ray tube). For TPD, the sample was cooled down typically to 110 K with liquid nitrogen before dosing any gas and then heated by radiation of a filament from behind at a constant rate of 1 K/s (digital temperature controller and power supply HS 130 and HS 720 of Schlichting Physikalische Instrumente).

As an option for sample cleaning, a radio frequency plasma cell (base pressure 10^{-7} mbar) was available from which samples could be directly transferred into the UHV chamber[32]. A treatment with oxygen plasma (25 W power with a continuous purge of 15 sccm O_2 at 4.5 mbar for 60 min.) and subsequent hydrogen plasma (20 W, 15 sccm H_2 at 4 mbar for 45 min.) was used for cleaning the sample surface in some experiments (see below). Other samples were submitted *ex-situ* to a continuous flow of oxygen containing 150 g/Nm^3 O_3 in a reactor tube at 470 K for two hours before transfer into UHV. This ozone treatment was employed as an alternative option to remove hydrocarbon contaminations and to oxidize the np-Au surface (see below).

TEM was performed in a FEI Titan 80/300 kV with imaging corrector (CEOS). TEM samples were prepared by ultra-microtomy of np-Au embedded in a polymer matrix. For SEM, a FEI dual beam (FIB/SEM) system was available.

Results

If not stated otherwise, experimental results reported in the following were obtained from activated np-Au samples that were neither heated nor cleaned in UHV. Heating was avoided (if not stated otherwise) in order to prevent any structural changes since the size of the ligaments and pores coarsens upon heating to temperatures above ~400 K[33] (cf. Fig. 1 d)). XPS of the outer surface of these samples shows, in addition to silver, residues of carbon and oxygen at coverages in a range equivalent to 1 ML. First, the interaction of CO with np-Au will be discussed, based on TPD experiments. Later, the focus will be shifted to oxygen species detected in and on np-Au and to the role that these may play for CO adsorption and chemistry.

Interaction of CO with npAu

Figure 2 shows TPD spectra of CO (upper panel) and CO_2 (bottom panel) obtained from two different but similarly prepared samples after dosing CO at 110 K. To sample "A" 100 L CO were dosed while 500 L were dosed to sample "B". CO desorption occurs for both samples in the temperature range between 120 and 240 K. Both spectra differ, however, with respect to the temperature of maximum desorption. Furthermore, more CO is desorbed from sample "A" than from sample "B" although five times more CO was dosed to sample "B".

Heating experiments indicate that these differences are most likely the result of surface contaminations by, e.g., volatile hydrocarbons. Figure 3 shows CO-TPD of sample "B" before and after heating to 900 K. Although the nanoporous morphology coarsened due to heating, the total amount of detected CO is higher after heating and the spectrum is qualitatively similar to that of sample "A"[33], suggesting that thermally induced desorption of surface contaminants has increased the number of adsorption sites for CO.

The spectra for samples "A" and "B" shown in Fig. 2 basically denote the range of results obtained from similarly prepared np-Au samples. Despite the noted differences, however, there are two distinct similarities which distinguish these spectra from those observed for single crystal gold surfaces. First of all, on np-Au we always find indication for at least *three* major CO desorption states in the range from 120 to 240 K. Second, desorption of the most stable CO species on np-Au at temperatures above 200 K is accompanied by CO_2 desorption.

In accordance with experimental and theoretical analysis of CO adsorption at single-crystal gold surfaces roughened by ion bombardment [34-36], CO desorption between 120 and 190 K

can be assigned to adsorption on Au at step and kink sites which are responsible for a typical fingerprint of two distinct CO desorption peaks in TPD. CO desorption above 200 K has been observed only in the case of Au(110)-(1x2) roughened by Ne^+ ion bombardment and only as minor species. It was related to the occurrence of low-coordinated Au sites as well[35]. In fact, nanosized gold particles which exhibit a high number of low coordinated surface atoms[37-39] show CO desorption at temperatures up to 300 K. As the particle size decreases, desorption peaks are shifted to higher temperatures possibly as a consequence of the particle size effect. A recent theoretical work showed that CO desorption above 200 K fits to CO adsorbed on a gold atom being in five-fold coordination (possibly stabilised by impurities) or to CO bound to Au atoms at step edges with adsorbed O adjacent to it[31].

The fact that CO_2 desorption is detected concomitantly with CO desorption in the range 200-240 K for samples freshly transferred from the reactor into the UHV-system implies that the np-Au samples already provide oxygen within a configuration that makes it available for CO oxidation in UHV at that temperature.

In order to find out whether all adsorbed CO species do react with the active oxygen species, in a second experiment the surface of sample "A" was exposed to CO at 175 K, i.e., above the temperature of desorption of CO species related to adsorption at Au step and kink sites (cf. Fig. 2). TPD shows CO_2 evolution in amounts similar to that observed before and directly correlated with the CO desorption above 200 K. Obviously, only that CO species being untypical of gold single crystal surfaces is oxidized.

In summary, np-Au features probably an atomic oxygen species at the surface (O_{act}) which is available for oxidation of CO. However, not all CO adsorbed on the surface can be oxidized by O_{act}, but only CO that desorbs above 200 K. What properties of np-Au that render it distinctly different from single-crystal gold surfaces are important for its capability to provide O_{act} and stable adsorption and reaction sites for CO? Before highlighting the role of oxygen, effects of the np-Au surface morphology, of silver residues, and of hydrocarbon or carbon deposits will be discussed in the following section.

Role of surface morphology, silver residues and other impurities

The curved ligaments of the sponge-like np-Au very likely feature a high density of low-coordinated gold sites which may be necessary for stable CO adsorption at temperatures above 200 K. Due to the ligament diameter being in the range of 50 nm, however, a multi-facetted surface appears to be a better model than that of a gold nanocluster (cf. Fig. 1 a)-c)). Given the fact that even Au(110) surfaces roughened by ion bombardment show CO

desorption above 200 K only as minor species, it appears unlikely that it is the nanoporous morphology *per se* which renders CO adsorption stable at temperatures above 200 K.

In our experiments we did not find any correlation between the amount of silver residues at the surface, varied by preparation of the np-Au from 6% to 20%, and the amount of CO desorption or CO_2 evolution above 200 K. Since CO is adsorbed on Ag much weaker than on the other noble metals Au and Cu[40-43], it can be excluded that CO adsorbs on Ag sites. Furthermore, DFT calculations found that silver as residue in the surface provides no significant stabilization of CO adsorption on gold. While silver probably plays a major role for oxygen adsorption on np-Au, the experiments indicate that it does not affect CO adsorption.

In order to elucidate the effect of surface contaminations, such as water, carbon or hydrocarbon species on CO adsorption, some samples were cleaned by oxygen and hydrogen plasma treatment (cf. experimental section). XPS revealed removal of carbon on the surface. CO-TPD showed a pronounced total increase of CO adsorption on plasma-cleaned np-Au while CO desorption was observed over the same temperature range as before, i.e., also above 200 K (see Fig. 4). In agreement with Fig. 3, the data thus indicate that residual carbon contaminants affect the CO adsorption predominantly by blocking adsorption sites on gold and not by providing new adsorption sites (in the neighbourhood, e.g.).

Oxygen Species on and in np-Au

Even without oxygen plasma or ozone treatment the activated np-Au surface exhibits several oxygen species, as revealed by XPS and TPD. Figure 5 shows photoelectron intensities in the range of the O 1s emission of an activated np-Au sample (top panel) and of that sample after heating (bottom panel). Care had been taken to ensure that only the np-Au and not any parts of the sample holder contributed to the spectra. Therefore, a gold foil was placed between sample and sample holder. The spectra were fitted by the program “fitt” with a Voigt profile (Hyun-Jo Kim, Department of Physics, Seoul National University). Two contributions are clearly seen. The one at ~530.2 eV binding energy fits to gold oxide (Au_2O_3), that one at 532.2 eV is in the range observed for hydroxides and carbonates on gold[44]. Fitting the O1s spectra and taking the sensitivity factor into account reveals an oxygen content of 15 – 30 % in the outer np-Au surface region visible for XPS.

For comparison, on Au(111) oxidized by ozone Min et al. identified three different oxygen species: chemisorbed atomic oxygen, ‘surface oxide’ and ‘bulk oxide’[45-47]. Chemisorbed oxygen showed no long range order but high mobility on the surface. At temperatures > 400

K this metastable species transforms into surface and bulk oxide. In scanning tunnelling microscopy the oxides were visible as two-dimensional and three-dimensional islands with crystalline order, respectively. On the basis of the desorption kinetics, Gottfried et al. also concluded for oxygen ion-bombarded Au(110) and Au(111) that islands and clusters are formed[48,49]. XPS yielded 530.1, 529.4, and ~529 eV as binding energies for bulk oxide, surface oxide, and chemisorbed oxygen, respectively. Chemisorbed atomic oxygen showed the highest activity towards CO oxidation compared to the surface oxide or the even less active bulk oxide.

In accordance, we assume that O_{act} , i.e., the oxygen species on np-Au consumed during CO oxidation, is chemisorbed atomic oxygen. The O1s binding energy of O_{act} on silver sites is expected at 528 – 529 eV[50-53] and, as mentioned before, on gold sites at ~529 eV[45-47]. Since both species found by XPS showed higher binding energies, none of them probably represents O_{act}. In an attempt to completely remove this active oxygen, np-Au samples were exposed to 10 mbar CO at room temperature for several hours. (Notably, even dosing amounts of CO (50000 L) that would be considered excessive with respect to planar surfaces, did not lead to a complete consumption of the active oxygen species on np-Au. Subsequent TPD spectra after dosing CO to the surface again still showed CO_2 evolution in the same range.) The active oxygen species could indeed be completely removed as confirmed by the absence of CO_2 desorption in a subsequent TPD of CO. XPS, however, showed no significant change of the O 1s spectrum, confirming that the XPS peaks at 530.2 and 532.2 eV binding energy represent inactive oxygen species that remain resident on the surface. Assuming that the XPS results obtained from the outer np-Au surface are also representative for the inner surface, we conclude that the density of the inactive oxygen species on the np-Au surface is much higher than that of O_{act}, being apparently a minority species.

Before discussing the nature of the inactive oxygen species and their role in the complex surface chemistry of npAu, more details on O_{act} shall be given first. When O_{act} was completely removed from the np-Au sample by exposure to CO and the sample was afterwards exposed to 10 mbar O_2 at RT for 3 h prior to a subsequent TPD experiment, again CO_2 evolution could be detected at the same temperature as before, revealing that O_{act} can reversibly be replenished on activated np-Au.

On samples that were not activated in the continuous flow reactor, O_{act} is also present directly after sample preparation and removed by exposure to 10 mbar CO. However, it cannot be replenished afterwards by exposure to 10 mbar O_2, as evidenced by missing CO_2 desorption

during a subsequent CO-TPD. In accordance, Wang et al. observed on *as-prepared* np-Au the formation of CO_2 in a TAP reactor during simultaneous pulses of CO and O_2 but the amount of CO_2 decreased continuously from pulse to pulse. While in their experiment active oxygen species are present on the surface at the beginning, no significant uptake or consumption of O_2 from the pulses was detected[54]. The initial presence of O_{act} on these samples is probably a consequence of the electrochemical dealloying process. Obviously, however, the *ex situ* activation procedure is necessary to change the surface in such a manner that O_2 dissociation is catalyzed even at room temperature.

Taking into account that adsorption and dissociation of O_2 probably take place on Ag sites at the surface (in contrast to Au, dissociative adsorption of oxygen has been reported for Ag single crystal surfaces at temperatures above 200 K[50-53]), it is likely that the *ex situ* activation procedure is a necessary step to expose a sufficient number of silver sites at the surface. Note that the CO desorption spectra obtained from the O_{act}-covered and from the O_{act}-depleted surface are exactly the same, suggesting that CO and O_{act} do not compete for the same adsorption sites, in agreement with the assumption that the adsorption of CO occurs on Au sites and O_{act} is generated on Ag sites (see also supplementary information S1).

In order to identify the oxygen species that are resident on the np-Au surface besides O_{act}, we performed TPD experiments, heating samples from 300 K up to 900 K. As expected, these experiments led to a coarsening of the sponge-like np-Au morphology, revealed by SEM (cf. Fig. 1 d))[33]. Three desorption peaks of molecular oxygen were detected in that temperature range (see Fig. 6). While the temperatures of the peak maxima varied for different samples, the first was always observed between 490 and 530 K, the second in the range of 550 to 630 K, and the third in the range 805 to 835 K.

Samples that were heated only to 550 K did not show any CO_2 desorption in a subsequent CO-TPD, indicating that O_{act} desorbs at ~510 K, probably after being transformed into other surface oxygen species. The temperature is characteristic for desorption of atomic oxygen from the surface of low-index single-crystal Au surfaces which is observed at 450-550 K, depending on the method with which the surfaces are oxidized[3,21,26,27,55]. On Ag(111) and on Ag(110) single crystal surfaces the associative desorption of atomic oxygen occurs at 580 K and at 600 K respectively[50-53], making an assignment to Ag sites less probable even when taking into account that Au destabilises the adsorption of O_{act} at adjacent Ag sites and may lead to lower desorption temperatures of O_{act} from such sites[56]. Thus, while we assume that the dissociative chemisorption of O_2, i.e., the formation of O_{act}, proceeds at Ag sites, it

appears likely that, at least when heating the sample to 550 K, chemisorbed atomic oxygen diffuses onto Au sites, in accord with the high surface mobility of atomic oxygen[46].

In our experiments we found a decrease of the O1s XPS signals at 530.1 eV and 532.2 eV after heating np-Au above 550 K, revealing that besides O_{act} probably also water, carbonates and resident gold oxide species on np-Au, inactive for CO oxidation, have desorbed. The TPD peaks at ~600 K and at ~825 K must represent at least two more oxygen species that are inactive with respect to CO oxidation up to room temperature. Therefore, we assume that they are related to subsurface oxygen or oxygen dissolved in the np-Au bulk, possibly embedded into the structure during the dealloying process. This interpretation is supported by the finding that the second and third desorption peak are absent after heating the sample to 900 K once and replenishing active oxygen by exposure to 10 mbar O_2 at room temperature (see supplem. inform. S2).

Gottfried et al. were able to generate such inactive oxygen species in single-crystalline gold surfaces as well by oxygen ion sputtering of Au(110)[26]. Desorption temperatures were found at 620 K and 680-830 K, respectively. The high-temperature peak shifted as the oxygen load or the ion energy was varied. Oxygen dissolved in silver showed similar behaviour.[57] The variation of oxygen desorption temperatures in our experiments from sample to sample may indicate different oxygen loads at subsurface np-Au or in the bulk. One may speculate that, compared to single-crystalline Au, the ability of np-Au to store oxygen underneath its surface may be enhanced due to the abundance of crystalline defects or lattice distortions in the nanosized ligaments. Theoretical calculations show that such subsurface oxygen species may be stable.[30,58] On the basis of XPS and O_2 TPD experiments with an oxidized np-Au surface (see supplem. inform. S3), we can exclude that desorption of O_2 at ~600 and ~825 K is correlated to a goldoxide species.

XPS shows (Fig. 5, bottom panel) that even after heating to 900 K, the peaks at 530.2 and 532.2 eV do not vanish, revealing a large reservoir of these species. Neither cleaning cycles with hydrogen plasma nor heating the np-Au close to its melting point (1200 K) could fully remove them in our experiments.

Although samples heated to temperatures above 550 K are no longer active for CO oxidation, even samples heated to 900 K show high-temperature CO desorption above 200 K. Experiments with np-Au treated by oxygen plasma or by ozone provide evidence that oxygen species on or in the np-Au surface are responsible for this stabilization of CO. Fig. 4 shows TPD spectra after dosing CO to a np-Au sample cleaned by subsequent oxygen and hydrogen

plasma (a) and after an additional treatment with oxygen plasma (b). While CO desorption above 200 K is observed in both cases, the oxidized surface shows a higher number of more strongly bound CO species and - compared to as-prepared activated np-Au (Fig. 2) - the desorption peaks are shifted to higher temperatures. Two different effects of surface or subsurface oxygen on the CO adsorption of np-Au can be conceived. As revealed by theoretical calculations, an oxygen atom adjacent to Au can withdraw electronic charge from the gold so that the σ-bond of CO to that Au atom is strengthened.[31] In addition to that, oxygen can stabilize Au atoms in sites of low coordination as demonstrated theoretically and in a scanning tunnelling microscopy study of oxygen ion-bombarded Au(111).[36,55,59-61] So, the catalytically inactive oxygen species have an important role in the complex surface chemistry of np-Au by stabilizing low coordinated Au sites and providing those adsorption sites for CO which are relevant for its oxidation.

Conclusions

The catalytic activity of np-Au for CO oxidation appears to be based on an unexpectedly complex interplay of gold, silver, CO, and several oxygen species on and in the surface. As also demonstrated before[14,15], residual silver is crucial for the ability of np-Au to dissociate and chemisorb molecular oxygen, rendering a presumably atomic oxygen species at the surface (O_{act}) available for CO oxidation. In comparison with recent work on as-prepared np-Au[54] we conclude that the initial activation step at elevated temperatures reported for np-Au catalysts[13-15,33] is required to render the np-Au surface capable of O_2 dissociation and O_{act} formation, probably by uncovering silver sites at the surface.

With respect to total amount, O_{act} is only a minor oxygen species at the surface, as our experiments revealed. XPS and TPD provided evidence for several inactive species that are not being consumed by oxidation reactions with CO, namely carbonates, gold oxide and in particular subsurface oxygen which is probably generated during production of np-Au by chemical leaching. The presence of the latter species, in part stable even up to the melting temperature of np-Au, seems to play a major role for the catalytic activity of np-Au: In comparison with pure gold surfaces, np-Au exhibits a pronounced additional CO desorption state at temperatures above 200 K. This desorption state alone represents CO which binds to np-Au strongly enough to react at significant rates with O_{act} before being desorbed, as shown by our TPD experiments. Recent theoretical studies demonstrated that the strong binding of

CO to np-Au cannot be explained by the presence of silver residues. It can be conceived, however, that it is induced by the formation of O-Au-CO complexes at low-coordinated surface sites. A combined theoretical and experimental study to elucidate the interaction of of subsurface oxygen and adsorbed CO at np-Au is under way.

Acknowledgement

Experimental support (SEM) by A. Zargham is gratefully acknowledged. Current address of A. Wittstock, Lawrence Livermore National Laboratory, NSCL, 7000 East Avenue, CA 94550, USA

Prepared by LLNL under Contract DE-AC52-07NA27344.

References

(1) Haruta, M. K., T.; Sano, H.; Yamada, N. *Chemistry Letters* **1987**, *16*, 405.

(2) Haruta, M. *Catalysis Today* **1997**, *36*, 153.

(3) Meyer, R.; Lemire, C.; Shaikhutdinov, S. K.; Freund, H. *Gold Bulletin* **2004**, *37*, 72.

(4) Pireaux, J. J.; Chtaib, M.; Delrue, J. P.; Thiry, P. A.; Liehr, M.; Caudano, R. *Surface Science* **1984**, *141*, 211.

(5) Sault, A. G.; Madix, R. J.; Campbell, C. T. *Surface Science* **1986**, *169*, 347.

(6) Valden, M.; Lai, X.; Goodman, D. W. *Science* **1998**, *281*, 1647.

(7) Lopez, N.; Norskov, J. K. *Journal of American Chemical Society* **2002**, *124*, 11262.

(8) Bondzie, V. A.; Parker, S. C.; Campbell, C. T. *Catalysis Letters* **1999**, *63*, 143.

(9) Tsubota, S.; Nakamura, T.; Tanaka, K.; Haruta, M. *Catalysis Letters* **1998**, *56*, 131.

(10) Schubert, M. M.; Hackenberg, S.; van Veen, A. C.; Muhler, M.; Plzak, V.; Behm, R. J. *Journal of Catalysis* **2001**, *197*, 113.

(11) Iizuka, Y.; Kawamoto, A.; Akita, K.; Date, M.; Tsubota, S.; Okumura, M.; Haruta, M. *Catalysis Letters* **2004**, *97*, 203.

(12) Sanchez-Castillo, M. A.; Couto, C.; Kim, W. B.; Dumesic, J. A. *Angewandte Chemie, International Edition* **2004**, *43*.

(13) Zielasek, V.; Jürgens, B.; Schulz, C.; Biener, J.; Biener, M. M.; Hamza, A. V.; Bäumer, M. *Angewandte Chemie* **2006**, *45*, 8241

(14) Wittstock, A.; B. Neumann; A. Schaefer; K. Dumbuya; C. Kübel; M. M. Biener; V. Zielasek; H.-P. Steinrück; J. M. Gottfried; J. Biener; A. Hamza; Bäumer, M. *The Journal of Physical Chemistry C* **2009**, *113*, 5593.

(15) Wittstock, A.; Zielasek, V.; Biener, J.; Friend, C. M.; Bäumer, M. *Science* **2010**, *327*, 319.

(16) Yin, H.; Zhou, C.; Xu, C.; Liu, P.; Xu, X.; Ding, Y. *Journal of Physical Chemistry C* **2008**, *112*, 9673.

(17) Zhang, J.; Ma, H.; Zhang, D.; Liu, P.; Tian, F.; Ding, Y. *Physical Chemistry Chemical Physics* **2008**, *10*, 3250.

(18) Zeis, R.; Lei, T.; Sieradzki, K.; Snyder, J.; Erlebacher, J. *Journal of Catalysis* **2007**, *253*, 132.

(19) Biener, J.; Nyce, G. W.; Hodge, A. M.; Biener, M. M.; Hamza, A. M.; Maier, S. A. *Advanced Materials* **2008**, *20*, 1211.

(20) Kramer, D.; Viswanath, R. N.; Weissmüller, J. *Nano Letters* **2004**, *4*, 793.

(21) Saliba, N.; Parker, D. H.; Koel, B. E. *Surface Science* **1998**, *410*, 270.

(22) Kim, J.; Samano, E.; Koel, B. E. *Surface Science* **2006**, *600*, 4622.

(23) Tsai, H.; Hu, E.; Perng, K.; Chen, M.; Wu, J. C.; Chang, Y. S. *Surface Science* **2003**, *537*.

(24) Koslowski, B.; Boyen, H. G.; Wilderotter, C.; Kästle, G.; Ziemann, P.; Wahrenberg, R.; Oelhafen, P. *Surface Science* **2001**, *475*, 1.

(25) Pireaux, J. J.; Chtaib, M.; Delrue, J. P.; Thiry, P. A.; Liehr, M.; Caudano, R. *Surface Science* **1984**, *141*, 221.

(26) Gottfried, J. M.; Elghobashi, N.; Schroeder, S. L. M.; Christmann, K. *Surface Science* **2003**, *523*, 89.

(27) Gottfried, J. M.; Schmidt, K. J.; Schroeder, S. L. M.; Christmann, K. *Surface Science* **2002**, *511*, 65.

(28) Liu, J.-H.; Wang, A.-Q.; Chi, Y.-S.; Lin, H.-P.; Mou, C.-Y. *Journal of physical Chemistry B* **2004**, *109*, 40.

(29) Jürgens, B.; Kübel, C.; Schulz, C.; Nowitzki, T.; Zielasek, V.; Biener, J.; Biener, M. M.; Hamaza, A. V.; Bäumer, M. *Gold Bulletin* **2006**, *40*.

(30) Moskaleva, L. V.; Zielasek, V.; Klüner, T.; Neyman, K. M.; Bäumer, M. *Chemical Physics Letters* **2012**, *525*, 87.

(31) Moskaleva, L. V.; Röhe, S.; Wittstock, A.; Zielasek, V.; Klüner, T.; Neyman, K. M.; Bäumer, M. *Physical Chemistry Chemical Physics* **2011**, *13*, 4529.

(32) Gehl, B.; U. Leist; V. Aleksandrovic; P. Nickut; V. Zielasek; H. Weller; K. Al-Shamery; Bäumer, M. *REVIEW OF SCIENTIFIC INSTRUMENTS* **2006**, *77*, 083902.

(33) Wittstock, A.; Wichmann, A.; Biener, J.; Bäumer, M. *Faraday Discussions* **2011**, *152*, 1.

(34) Ruggiero, C.; Hollins, P. *Journal of the Chemical Society, Faraday Transactions articles* **1996**, *92*, 4829.

(35) Gottfried, J. M.; Schmidt, K. J.; Schroeder, S. L. M.; Christmann, K. *Surface Science* **2003**, *536*, 206

(36) Yim, W. L.; Nowitzki, T.; Necke, M.; Schnars, H.; Nickut, P.; Biener, J.; Biener, M. M.; Zielasek, V.; Al-Shamery, K.; Klüner, T.; Bäumer, M. *Journal of Physical Chemistry C* **2007**, *111*, 445.

(37) Lemire, C.; Meyer, R.; Shaikhutdinov, S. K.; Freund, H.-J. *Surface Science* **2004**, *552*, 27.

(38) Shaikhutdinov, S. K.; Meyer, R.; Naschitzki, M.; Bäumer, M.; Freund, H.-J. *Catalysis Letters* **2002**, *86*, 211.

(39) Zhao, Z.; Diemant, T.; Rosenthal, D.; Christmann, K.; Bansmann, J.; Rauscher, H.; Behm, R. J. *Surface Science* **2006**, *600*, 4992.

(40) Bradshaw, A. M.; Pritchard, J. *Proceedings of the Royal Society (London)* **1970**, *169*, A316.

(41) Browker, M.; Barteau, M. A.; Madix, R. J. *Surface Science* **1980**, *92*, 528.

(42) McElhiney, G.; Papp, H.; Pritchard, J. *Surface Science* **1976**, *54*, 617.

(43) Lee, J.; Lee, J.-G.; Yates Jr., J. T. *Surface Science* **2005**, *594*, 20.

(44) Irissou, E.; Denis, M. C.; Chaker, M.; Guay, D. *Thin Solid Films* **2005**, *472*, 49.

(45) Min, B. K.; Alemozafar, A. R.; Pinnaduwage, D.; Deng, X.; Friend, C. M. *Journal of Physical Chemistry B* **2006**, *110*, 19833.

(46) Min, B. K.; Friend, C. M. *Chemical Reviews* **2007**, *107*, 2709.

(47) Baker, T. A.; Liu, X.; Friend, C. M. *Physical Chemistry Chemical Physics* **2010**, *13*, 34.

(48) Gottfried, J. M.; Schmidt, K. J.; Schroeder, S. L. M.; Christmann, K. *Surface Science* **2003**, *525*, 184.

(49) Gottfried, J. M.; Schmidt, K. J.; Schroeder, S. L. M.; Christmann, K. *Surface Science* **2003**, *525*, 197.

(50) Campbell, C. T. *Surface Science* **1986**, *173*, L641.

(51) Besenbacher, F. *Surface Science* **1993**, *44*, 5.

(52) Campbell, C. T. *Surface Science* **1985**, *157*, 43.

(53) Campbell, C. T.; Paffett, M. T. *Surface Science* **1984**, *143*, 517.

(54) Wang, L. C.; Jin, H. J.; Widmann, D.; Weissmüller, J.; Behm, R. J. *Journal of Catalysis* **2011**, *278*, 219.

(55) Min, B. K.; Alemozafar, A. R.; Biener, M. M.; Biener, J.; Friend, C. M. *Topics in Catalysis* **2005**, *36*, 77.

(56) Kondarides, D. I.; Verykios, X. E. *Journal of Catalysis* **1996**, *158*, 363.

(57) Rehren, C.; Isaac, G.; Schlögl, R.; Ertl, G. *Catalysis Letters* **1991**, *11*, 253.

(58) Baker, T. A.; Xu, B. J.; Liu, X. Y.; Kaxiras, E.; Friend, C. A. *J. Phys. Chem. C* **2009**, *113*, 16561.

(59) Min, B. K.; Deng, X.; Pinnaduwage, D.; Schalek, R.; Friend, C. M. *Physical Review B* **2005**, *72*.

(60) Biener, J.; Biener, M. M.; Nowitzki, T.; Hamza, A. V.; Friend, C. M.; Zielasek, V.; Bäumer, M. *Chemphyschem* **2006**, *7*, 1906.

(61) Baker, T. A.; Liu, X. Y.; Friend, C. M. *PCCP* **2011**, *13*, 34.

Figures

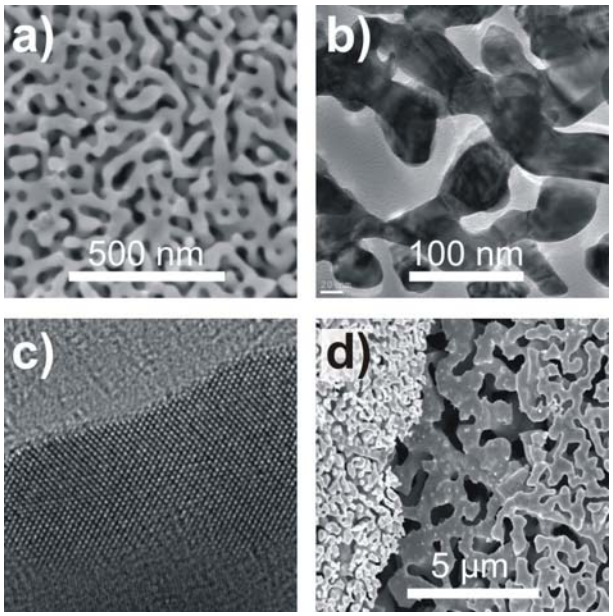

Figure 1: a) SEM of the surface of freshly prepared, activated np-Au; b) TEM of a sample cross section produced by microtomy; c) HRTEM detail of b); d) SEM at a crack of np-Au heated to 900 K, revealing heat-induced coarsening of the ligaments.

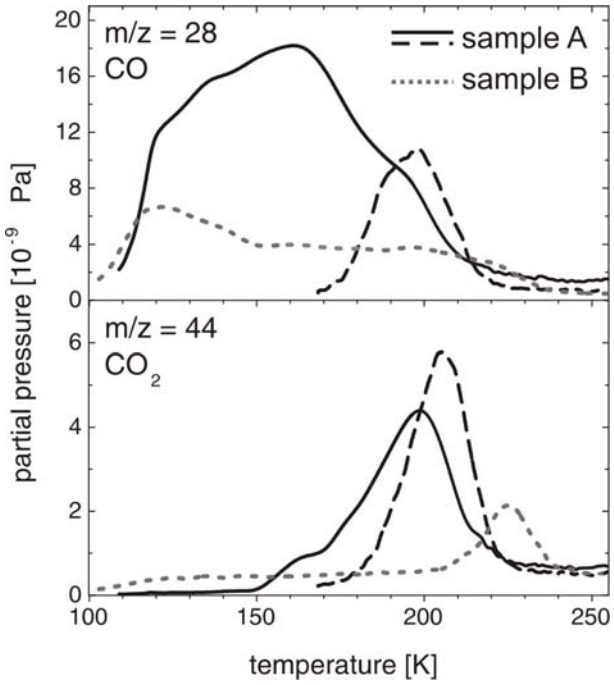

Figure 2: TPD of CO (m/z=28, top panel) and CO_2 (m/z=44, bottom panel) after exposing two freshly prepared, activated np-Au to CO at T=105 K: 100 L CO for sample A (solid black lines) and 500 L CO for sample B (dotted grey lines). In both cases CO desorption occurs between 110 and 240 K. The presence of CO_2 desorption reveals active oxygen on the surfaces which reacts with CO at above 200 K. Also shown: CO and CO_2 desorption after dosing 100 L CO to sample A at 176 K (dashed black line). Similar amount of CO_2 as after dosing CO at 110 K indicates that only the CO species desorbing at ~200 K and above is oxidized. All spectra were recorded at a constant heating rate of 1 K/s.

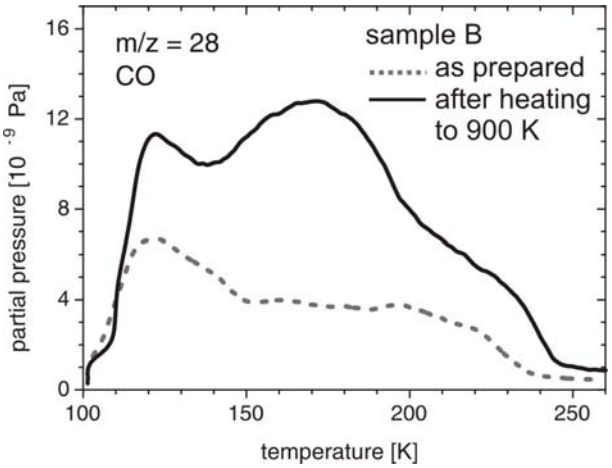

Figure 3: TPD after exposuring 500 L CO at 105 K to sample B as prepared (activated in the continuous flow reactor and transferred into UHV, dotted line, cf. Fig. 1) and after heating to 900 K (solid line). Increase of CO desorption indicates unblocking of CO desorption sites probably by removal of surface contamination.

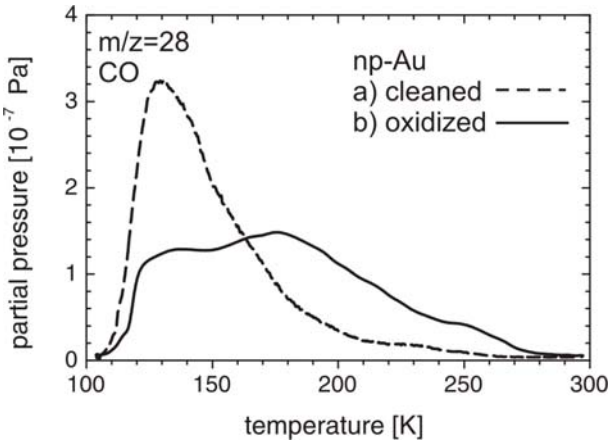

Figure 4: CO-TPD (m/z = 28, heating rate 1 K/s) after dosing 500 L CO at 105 K to a np-Au sample a) cleaned by subsequent oxygen and hydrogen plasma (dashed line) and b) oxidized by an additional oxygen plasma treatment for 30 min (solid line).

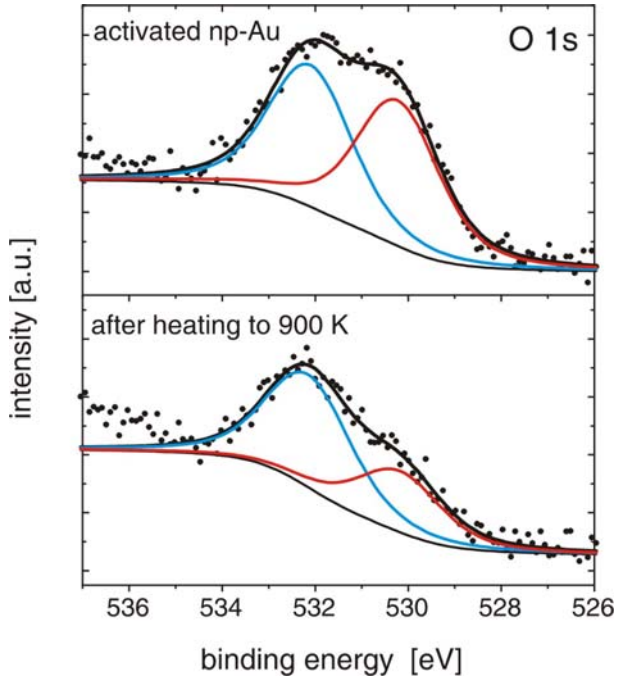

Figure 5: O 1s photoemission spectra obtained from the sample activated in the continuous flow reactor (bottom panel) and after heating the sample to 900 K (top panel). The loss of O 1s intensity is not due to desorption of O_{act} or the other inactive species, but rather due to desorption of CO_2.

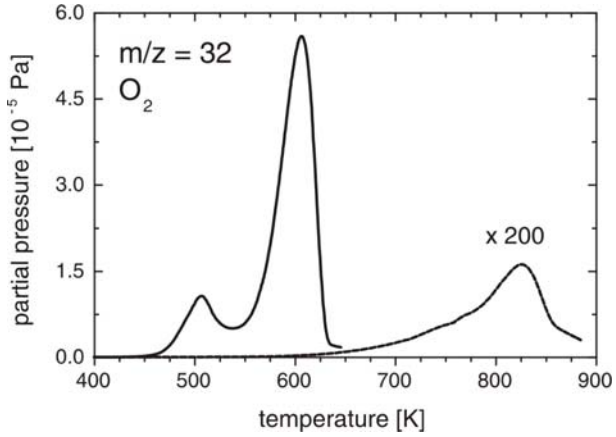

Figure 6: Two subsequent TPD experiments (heating rate 1 K/s) recording O_2 desorption (m/z=32) at 510 and 610 K (first run, heating up to 640 K) and at 830 K (second run, heating up to 900 K), obtained after reactivating O_{act}-depleted np-Au by exposure to 10 mbar O_2 at 300 K. O_{act} desorbs at ~510 K (see text for details).